Version of Record: https://www.sciencedirect.com/science/article/pii/S0926860X23001370
Manuscript_779371652b719bb46d116a30ba116167

Strategies for Regeneration of Pt-alloy Catalysts Supported on Silica for Propane Dehydrogenation

Ryan Alcala[1], David P. Dean[2], Isha Chavan[2], Che-Wei Chang[2], Brandon Burnside[1], Hien N. Pham[1], Eric Peterson[1], Jeffrey T. Miller[2,*], and Abhaya K. Datye[1,*]

[1]Department of Chemical and Biological Engineering and Center for Microengineered Materials, University of New Mexico, Albuquerque, New Mexico 87131, USA

[2]Davidson School of Chemical Engineering, Purdue University, 480 Stadium Mall Drive, West Lafayette, IN 47907-2100, USA

[*]Address for correspondence and proofs: datye@unm.edu

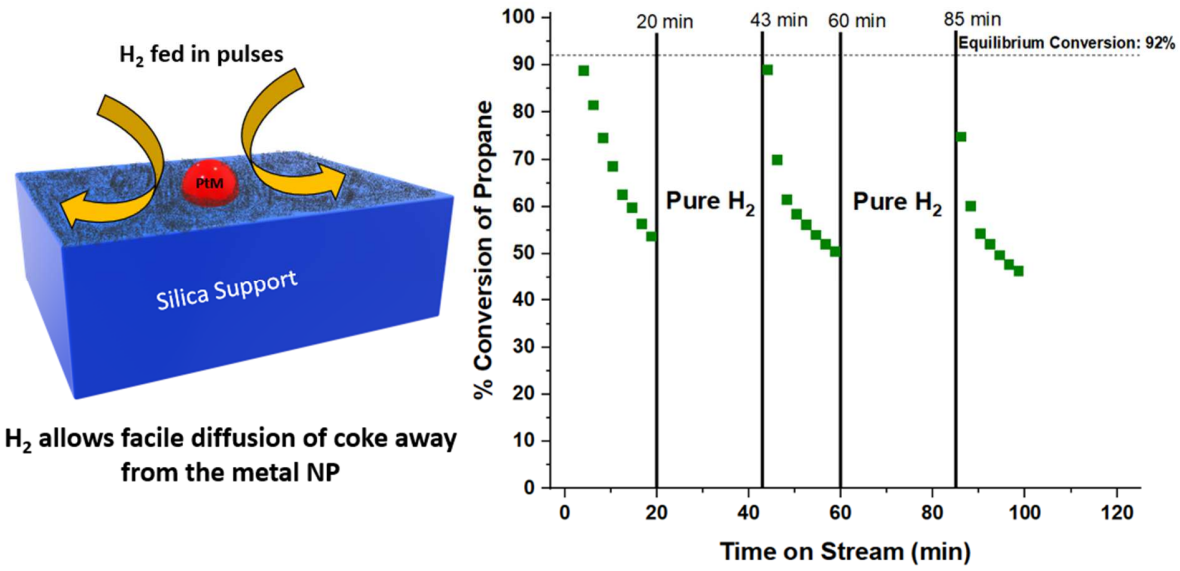

Abstract

Catalyst stability, resistance to deactivation, and regeneration remain a challenge for high temperature reaction processes. For Pt alloys used in propane dehydrogenation (PDH), the primary pathways of catalyst deactivation include coke formation and metal nanoparticle sintering over time. Recent work shows that silica-supported catalysts provide excellent selectivity for this reaction, but the regenerability of silica-supported catalysts has not been established. In this work, we study a series of Pt alloys, including PtMn, PtZn, and PtSn, for the PDH reaction at 550 °C and 600 °C, and we subject the catalyst materials to regeneration over multiple cycles. While oxidation in air restores the reactivity completely with minimal catalyst sintering, it is surprising to find that these catalysts can also be regenerated in pure hydrogen. Here we explore the types of coke formed on these catalysts using *in situ* temperature programmed oxidation (TPO). Two types of coke are found: one on the metallic NP surface, and a second on the silica support. Our work shows that treatment in hydrogen causes redistribution of the coke between the metal and support, which can restore most catalytic activity lost during a reaction run. Periodic introduction of H_2 during a reaction cycle may constitute an unexplored strategy for extending the lifetime of PDH catalysts.

1. Introduction

The "Shale Boom" has provided a large feedstock of hydrocarbon resources that have a high hydrogen to carbon ratio, and the extraction of shale gas in the U.S. is projected to increase until at least 2050 [1–3]. Conversion of the natural gas liquids obtained from shale, *e.g.* ethane and propane, involves dehydrogenation as the first step [4]. The product alkenes, ethylene and propylene, are precursors for a variety of useful compounds including chemical derivatives and liquid transportation fuels. However, methane, ethane, and propane, the major components of natural gas, are difficult to activate, and dehydrogenation is a highly endothermic, equilibrium-limited reaction. Conventionally, Pt alloys or CrO_x based catalysts supported on alumina have been employed for commercial dehydrogenation [5,6]. Pt catalysts are the most prominent materials for non-oxidative dehydrogenation. An additional element, called a promoter, is often added to form a Pt alloy in order to modify the geometric and electronic structure of the Pt surface ensembles to increase the selectivity of the catalyst. Conventionally, a Pt_3Sn alloy supported on Al_2O_3 is used in the industrial process (UOP Oleflex process) [5,6]. Nevertheless,

the Pt_3Sn catalyst deactivates and requires frequent regeneration [7]. The mechanisms for deactivation include sintering of metal nanoparticles, coking of catalyst active sites, and the transformation of the active surface phase by loss of promoters [6,8]. Methods for catalyst regeneration on alumina supported catalysts are well developed and, in fact, commercial processes are designed around a regenerative protocol involving fluidized beds (Dow FCDh© process), alternating reactors (Lummus Catofin© process), or a moving bed that undergoes continuous regeneration (UOP Oleflex© process) [5,9].

Commercial processes for PDH may operate anywhere from seconds to days before requiring oxidative regeneration to remove coke from the catalyst [5]. Across numerous periodic reductive/oxidative regenerative cycles at high temperatures, the industry standard Pt_3Sn/Al_2O_3 deactivates as Sn leaches out of the alloy, forming a separate SnO_x phase elsewhere on the support [7,10]. Additionally, the rigorous regenerative cycles cause sintering of nanoparticles, which causes the loss of active sites as nanoparticles agglomerate [11]. Therefore, it is beneficial to explore strategies for prolonging or completely avoiding high temperature oxidative regeneration, which is one of the goals of this work. Previous studies, both computational and experimental, have shown that when hydrogen is co-fed for PDH over a Pt catalyst (and other materials), the catalyst exhibits higher activity and stability [12–20]. It is known that this strategy has been implemented commercially [21]. Propane dehydrogenation is an equilibrium-driven reaction so the reaction performed with cofed H_2 has a lower maximum possible conversion that one without cofed H_2. When operating below maximum possible conversion for a reaction, it is observed that H_2 actually increase selectivity which consequently improves stability and even the site time yield of the catalyst. This form of coke suppression attributed to the increase in hydrogen partial pressure leads to a lower coverage of deeply dehydrogenated precursors on the surface (i.e., CCH_3 ethylidyne and CH methylidyne) by competing for active sites and preventing the readsorption of nascent propylene. Additionally, the higher the hydrogen coverage, the lower the propylene adsorption strength and the higher the energy barrier for further dehydrogenation of propylene [12]. Siddiqi *et al.* explore the role of hydrogen partial pressure on dehydrogenation activity and selectivity for a Pt-Ga alloy catalyst. The study compared PDH to ethane dehydrogenation (EDH) and experimentally determined that the rate of formation of propylene and ethylene, respectively, achieved a maximum with respect to hydrogen/hydrocarbon feed ratio. The authors propose, by analyzing coking rates of EDH and

PDH while co-feeding hydrogen, that for PDH most of the coke resides on the support with minimal coverage of the catalyst surface [13]. The remarkable and counterintuitive effect of increasing dehydrogenation catalyst stability and activity by co-feeding hydrogen is well-established and suggests that a strategy could be developed whereby hydrogen can be used to regenerate Pt-alloy dehydrogenation catalysts.

Here, we propose a strategy where harsh, high temperature oxidative catalyst regeneration treatments can be avoided to improve catalyst stability. Catalyst regeneration using hydrogen can circumvent conditions which lead to long-term catalyst deactivation such as sintering and phase segregation [5]. Alleviating the need for frequent oxidative regeneration also simplifies the design and operation of the process. Nonetheless, co-feeding hydrogen limits equilibrium conversion, so the ratio of hydrogen to alkane feed should be optimized to balance stability and high yield [13]. Our proposed strategy involves cofeeding hydrogen to the catalyst either continuously or in pulses, providing an alternative approach to industrial propane dehydrogenation. In addition to the industrial standard, Pt_3Sn, we are studying two alloy catalysts, Pt_3Mn and Pt_1Zn_1, to assess the new operational approach. An optimal alloy composition and synthesis procedure was formulated based on the groups' previous experience synthesizing and characterizing these catalyst materials [22–29]. Pt_3Mn was selected because of its stable performance for EDH where it lost no activity over the course of a week [26]. Pt_1Zn_1 was selected because its body-centered cubic (BCC) structure forms site-isolated Pt atoms on the alloy surface. This results in a highly selective PDH catalyst which differs from the three-fold Pt ensembles characteristic of the face-centered cubic (FCC) Pt_3Mn and Pt_3Sn material surfaces [25]. Typically, catalysts used in commercial processes are supported on alumina due to thermal stability, high surface area, and the ability to regenerate the catalyst oxidatively [6,7]. However, recent work shows that silica supports may provide higher propylene selectivity for PDH as well as lower coke formation and catalyst deactivation rates [30–32]. Coking and cracking side reactions on alumina occur via C-C bond activation and C-H bond overactivation at Lewis acid sites on the alumina surface that can be formed at high temperature under reducing conditions [33–36]. Commercially, basic promoters such as Na, K, or Ca are commonly used to block sites on alumina that lead to coke formation, albeit at the cost of some catalytic activity [37]. Silica has fewer Lewis acid sites, and thereby has lower coking rates. Despite improvements in

selectivity and stability using silica supports, the regenerability of silica-supported dehydrogenation catalysts has not been well established. [16,20,30,36,38–42].

Many studies assess PDH catalyst stability during a single reaction run, typically on the order of days, but often disregard the aspect of catalyst regeneration, which is important to the design of industrial PDH catalysts [25,36,43–46]. Other recent studies that explore catalyst regeneration often employ a high temperature oxidative treatment that irreversibly deactivates the catalyst [7,16,19,20,23,47,48]. A previous study by Deng *et al.* explores regenerating a $PtSn/SiO_2$ catalyst using pure hydrogen at 800 °C [31]. However, PtSn nanoparticles supported on alumina are reported to sinter upon reductive treatment at significantly lower temperatures [49](above 600 °C), meaning that the catalyst likely sinters and irreversibly deactivates between reaction runs, making the treatment difficult to assess. Another previous study by Sun *et al.* reports regenerating a $PtSn/\gamma\text{-}Al_2O_3$ catalyst using pure hydrogen as a more effective method for catalyst regeneration compared to oxidative or inert regeneration. Nevertheless, the study only reports a decrease in catalyst activity after hydrogen regeneration treatment at 540 °C for each cycle [50]. This study will employ a highly selective and stable Pt-alloy material supported on silica as a PDH catalyst to probe the possibility of using hydrogen as an alternative regeneration treatment to oxidative conditions. We aim to address the role hydrogen plays in stabilizing and regenerating the catalysts by assessing reaction performance as well as the distribution of coke on the catalyst surface across multiple reaction cycles.

2. Experimental Methods

Catalyst Synthesis

First, the method of strong electrostatic adsorption method (SEA) was used on 5 g of commercially available silica (Sigma- Aldrich, Davisil grade 646) to prepare Zn/SiO_2. 0.68 g of $Zn(NO_3)_2{\cdot}6H_2O$ (Sigma-Aldrich) was dissolved in 50 mL of deionized water (DI water) to obtain 3% Zn weight loading. Subsequently, ammonium hydroxide (NH_4OH, Sigma-Aldrich) was added to a $Zn(NO_3)_2$ solution to adjust the pH to 11−12. SiO_2 was added to the Zn solution and stirred for 10 min. The sample was vacuum filtered and washed with 50 mL of DI water three times. The wet powder was dried overnight at 125 °C and calcined at 300 °C for 3 h (10 °C/min). Pt was then added to Zn/SiO_2 by the pH adjusted incipient wetness impregnation

method (IWI) to give 2% Pt weight loading in the final $PtZn/SiO_2$ catalyst. Its impregnation volume was calculated to be 1.16 mL/g by adding H_2O dropwise to 1g of SiO_2 until it was saturated. Here, 0.2 g of $Pt(NH_3)_4(NO_3)_2$ (Sigma-Aldrich) was dissolved in about 2 mL of DI water. Then, 1 mL of NH_4OH was added to the Pt solution and stirred until all crystals dissolved. Water and NH_4OH were added until the volume was sufficient to impregnate the pore volume of the SiO_2 and the pH of the Pt solution was between 11−12. The solution was added dropwise to the Zn/SiO_2 support while stirring. The catalyst was dried overnight at 125 °C, calcined at 200 °C for 3 hr (5 °C/min ramp), and reduced at 225 °C in 5% H_2/N_2 at 100 cm^3/min for 30 min [22,51,52]. A similar approach was used to prepare PtMn and PtSn catalysts on silica using $Mn(NO_3)_2 \cdot 4H_2O$ (Sigma-Aldrich) and $SnCl_4 \cdot 5H_2O$ (Sigma-Aldrich), respectively. The weight loadings for $PtZn/SiO_2$ (2 wt% Pt, 3 wt% Zn), $PtMn/SiO_2$ (2 wt% Pt, 5 wt% Mn), and $PtSn/SiO_2$ (2 wt% Pt, 1.5 wt% Sn). Alloy formation was confirmed by *in situ* XAS.

Brunauer-Emmett-Teller (BET) Analysis

BET analysis of all samples was performed using a Micromeritics Gemini 2360 Surface Area Analyzer, using liquid nitrogen coolant, after a 24-hr degassing period at 120 °C under flowing nitrogen gas.

X-ray Diffraction (XRD)

X-ray diffraction data was collected using a Rigaku SmartLab powder x-ray diffractometer, equipped with a Cu-target X-ray source (40 kV, 40 mA), a D/TeX Ultra 1-dimensional position sensitive detector, and a Ni-foil filter for reduction of the Cu-Kβ component of the diffracted radiation. Data was collected at 6 °/min from 3° to 150° 2θ (0.02° step size). Lattice parameters were obtained via Rietveld refinement using the MDI Jade software package. Lattice parameters, crystallite size, and micro strain values were refined, as well as sample height error.

Transmission Electron Microscopy (TEM)

Samples were dispersed in ethanol and mounted on holey carbon grids for examination the JEOL NeoARM 200CF transmission electron microscope equipped with a spherical aberration corrector to allow atomic resolution imaging and an Oxford Aztec Energy Dispersive

System (EDS) for elemental analysis. The microscope is equipped with two large area JEOL EDS detectors for higher throughput in the acquisition of X-ray fluorescence signals. Images were recorded in annular dark field (ADF) mode and in annular bright field (ABF) mode.

X-ray Absorption Spectroscopy (XAS)

In situ XAS experiments were performed at the MR-CAT 10-BM beamline at the Argonne APS and the 8-ID ISS beamline at the Brookhaven NSLS-II [53]. The catalyst materials were scanned at the Pt L_3 edge (11.564 keV) for the $PtSn/SiO_2$, $PtMn/SiO_2$, and $PtZn/SiO_2$ samples. Samples were ground to a fine powder and packed into a sample holder. The sample holder was placed in an *in situ* cell in the middle of a quartz tube with leak-tight end caps containing X-ray-transparent Kapton windows. All the samples were placed into the same cell for simultaneous analysis. The samples were reduced in 5% H_2/He at 550 °C for 30 minutes, then cooled to 25 °C in He and scanned. Sample measurement was accompanied by a Pt foil scan, used for energy calibration, which was obtained simultaneously using a third ion chamber. The X-ray absorption near edge structure (XANES) spectra were used to identify the oxidation state while the extended X-ray absorption fine structure (EXAFS) provided information about the number, identity, and distance of local scattering atoms. XANES and EXAFS data were obtained and interpreted using WinXAS v 4.0 software.[54] Feff6 calculations were performed using a single scattering atom of each type placed at a certain distance from a main Pt atom. [55] The type of atom and distance is as follows: Pt–Zn = 2.66 Å, Pt–Pt = 2.77 Å, Pt–Mn = 2.66 Å, Pt–Sn = 2.81 Å, Pt–O = 2.05 Å. The standard EXAFS fit was performed on the k^2-weighted, Fourier-transform of the reduced (metallic) sample.

In order to assess the local coordination at the surface of the nanoparticles, we employed difference-EXAFS (surface-EXAFS) analysis on the samples [26,56,57]. After scanning the reduced sample, we re-exposed the sample to air (oxidative treatment) at room temperature for 30 minutes before scanning the sample a second time. At room temperature in air the surface layer(s) of Pt will oxidize. Upon subtracting the k^0-weighted χ-space spectra of the reduced and surface-oxidized spectra, the core of the nanoparticles (the portion that did not change) is

subtracted out, meaning that only the contribution of the atoms near the surface remains. The data was fitted using the scattering paths listed above; however, the phase of the Pt-O scattering path was shifted π-radians out of phase compared to conventional EXAFS.

Reaction Testing

Reaction conditions are defined throughout the results section because of the variety of conditions used. The most common conditions, however, are termed as "coking conditions" and "non-coking conditions". Coking conditions indicates 5% propane in balance Ar at 550 °C while non-coking conditions indicates H_2 cofeeding in ratios that are typically 1:1 or 2:1 with respect to propane at 550 °C or 600°C.

Results

The samples prepared for this study were characterized using XAS. The samples were pre-reduced in 5% H_2/He at 550 °C for 30 minutes before cooling to room temperature in He and scanning in transmission mode. Figures S1 and S2 show the XANES and the EXAFS for the Pt alloy catalysts, respectively. For the pre-reduced scans, the EXAFS shows no evidence of Pt-O features, which commonly appears lower than R = 1.8 Å, meaning that the alloy nanoparticles are fully metallic. The XANES energy, defined as the inflection point of the initial photoexcitation, increased with alloy formation by ~0.5 eV, listed in Table 1, compared to the Pt foil. This shift is consistent with alloy formation [25,26]. The EXAFS spectra show a noticeable difference in magnitude and peak position for each alloy compared to the Pt foil reference, which has three peaks. This suggests scattering paths other than Pt-Pt, and the small magnitude may be attributed to destructive interference between the scattering paths. EXAFS fitting results are reported in Table 1 and Figure S3. Upon fitting, the PtZn/SiO_2 sample had a Pt-Zn scattering path present at a bond distance longer than a Pt-Pt scattering path, which is typical of a Pt_1Zn_1 structure previously reported [22,25,58]. The ratio of Pt-Pt bonds to Pt-Zn bonds is approximately 3:1, suggesting the formation of Pt-rich nanoparticles, i.e., a Pt core and surface Pt_1Zn_1 phase. For the PtMn/SiO_2 catalyst, the Pt-Pt:Pt-Mn coordination ratio is approximately

3:1, and the bond distance is the same between both scattering paths at a bond distance slightly shorter than that of Pt-Pt [26]. This suggests the formation of Pt-rich nanoparticles containing a Pt_3Mn phase because the Pt-Pt:Pt-Mn coordination ratio, 3:1, is higher than the expected 2:1 ratio for full-alloy Pt_3Mn nanoparticles. Using similar logic for the $PtSn/SiO_2$ sample, the Pt-Pt:Pt-Sn coordination ratio is approximately 3:1, which points to Pt-rich nanoparticles containing a Pt_3Sn phase. The bond distance found for Pt-Pt and Pt-Sn coordination in the $PtSn/SiO_2$ sample is significantly longer (~0.1 Å) compared to monometallic Pt nanoparticles of this size (~2 nm in diameter), which is attributed to the formation of a Pt_3Sn phase [59]. The bond distance extension is confirmed using XRD, as evidenced by a spectral shift to lower 2θ in Figure S5.

Table 1. Pt L_3 edge EXAFS fits for the $PtZn/SiO_2$, $PtMn/SiO_2$, and $PtSn/SiO_2$ samples.

Sample	Edge energy (keV)	Scattering Pair	CN (±10%)	R (±0.02 Å)	$\Delta\sigma^2$ (Å^2)	Shift in E_o (eV)
Pt foil	11.5640	Pt-Pt	12.0	2.76	-	6.3
re-2Pt-3Zn	11.5647	Pt-Pt	5.3	2.71	0.005	2.1
		Pt-Zn	1.6	2.52	0.005	-2.0
re-2Pt-5Mn	11.5644	Pt-Pt	6.0	2.68	0.004	2.9
		Pt-Mn	2.0	2.69	0.004	3.4
re-2Pt-1.5Sn	11.5647	Pt-Pt	6.1	2.77	0.004	0.1
		Pt-Sn	1.9	2.75	0.004	5.2

To determine whether the alloy phase or the Pt-rich phase is on the surface of the nanoparticles, difference-EXAFS (surface-EXAFS) analysis was used. By subtracting a sample's partially oxidized spectra from a fully metallic spectra, considering that the core stays the same and the atoms near the surface change, information about element-specific local coordination closer to the surface of the nanoparticles can be procured. The resulting fits are listed in Table 2 and are illustrated in Figure S4. The difference between the reduced and oxidized spectra is represented as a loss of Pt-Pt and Pt-(Sn, Zn, Mn) coordination and a gain of Pt-O coordination. Both the gained coordination and lost coordination are accounted for in difference EXAFS fitting results. The results show that a large proportion of the $PtZn/SiO_2$ sample oxidized upon exposure to air at room temperature, but the metallic coordination change near the surface has a Pt-Pt:Pt-Zn coordination ratio of 3.5:1.9, which is lower than in the bulk fitting results above. This shows that there is more Zn near the surface of the nanoparticles meaning a Pt-Zn surface alloy phase.

The $PtMn/SiO_2$ and even less so the $PtSn/SiO_2$ sample were minimally oxidized upon exposure to air at room temperature. The metallic coordination change near the surface has a Pt-Pt:Pt-Mn and Pt-Pt:Pt-Sn ratio of approximately 2:1 for both materials. This is higher than the bulk ratio, and again conveys the formation of a Pt-Mn or Pt-Sn surface alloy phase. The ratio of 2:1 specifically aligns with the formation of either a Pt_3Mn or Pt_3Sn phase, which coincides with expectations based on the chosen synthesis procedures. It should be noted that because this difference fitting analysis involves the subtraction of two EXAFS spectra, small structural differences are being assessed and the error is therefore higher compared to bulk EXAFS fitting.

Table 2. Pt L_3 edge surface-EXAFS fits for the $PtZn/SiO_2$, $PtMn/SiO_2$, and $PtSn/SiO_2$ samples.

Sample	Scattering Pair	CN (±20%)	R (±0.04 Å)	$\Delta\sigma^2$ (Å^2)	Shift in E_o (eV)
re-2Pt-3Zn	Pt-Pt	3.5	2.73	0.005	-3.5
	Pt-Zn	1.9	2.50	0.005	4.0
	Pt-O	1.8	1.98	0.001	0.1
re-2Pt-5Mn	Pt-Pt	2.1	2.73	0.004	-6.8
	Pt-Mn	0.9	2.68	0.004	2.4
	Pt-O	0.4	1.99	0.001	-3.4
re-2Pt-1.5Sn	Pt-Pt	1.1	2.81	0.004	-7.3
	Pt-Sn	0.6	2.73	0.004	5.8
	Pt-O	0.3	1.98	0.001	-2.1

Figure 1A shows the propane dehydrogenation reactivity of the Pt-Zn catalyst for 5 cycles involving ~1000 minutes of reaction. After each reaction cycle, oxidative regeneration was performed with air at 420°C for 1 hour. The role of added hydrogen (H_2:C_3H_8 = 0,1, or 2) on the deactivation rate was studied for propane dehydrogenation (10% propane in Ar) on the $PtZn/SiO_2$ catalyst using a WHSV of 11.4 g propane/g catalyst/hr at 550°C. As seen in Figure 1A, without added hydrogen, the catalyst loses conversion and deactivates rapidly during the first three reaction cycles, which are each 18 hours long. The fact that the catalyst regains its initial conversion at the beginning of each cycle (after regeneration) implies that the catalyst can be regenerated oxidatively without sintering of the alloy NPs. Cycle 4 and Cycle 5 involve co-feeding hydrogen in a ratio of H_2:C_3H_8 = 1 and 2 respectively. Figure 1A shows the extent of

single-cycle deactivation during cycles 4 and 5 was much less pronounced than cycles 1-3. Cycle 5 provided stable operation, achieving 84% of equilibrium conversion at the end of the 20-hour run. By contrast, in cycles 1-3 with no added hydrogen, the catalyst reached about 25% of equilibrium conversion at the end of ~ 20 hours of operation. These results demonstrate that co-feeding hydrogen improves catalyst stability and achieves long-term operation closer to equilibrium. After 5 cycles, the catalyst was removed from the reactor for examination by electron microscopy. The HAADF STEM images in Figure 1B show that the catalyst particle size distribution remains, within experimental error, unchanged after 5 reaction/oxidation/re-reduction cycles, indicating that the silica supported PtZn catalyst can be oxidatively regenerated without causing sintering of the NPs, implying that sintering is not the primary deactivation mechanism. Figure S6, S7, and S8 show EDS mapping of the PtMn catalyst after reaction, reduction, and oxidation showing both components in a homogenous mixture. The initial composition by SEM/EDS is 2.3% Pt and 3.2% Zn, by weight, as seen in Figure S9. Figure S10 contains a similar plot demonstrating the regenerability of $PtSn/SiO_2$ in air.

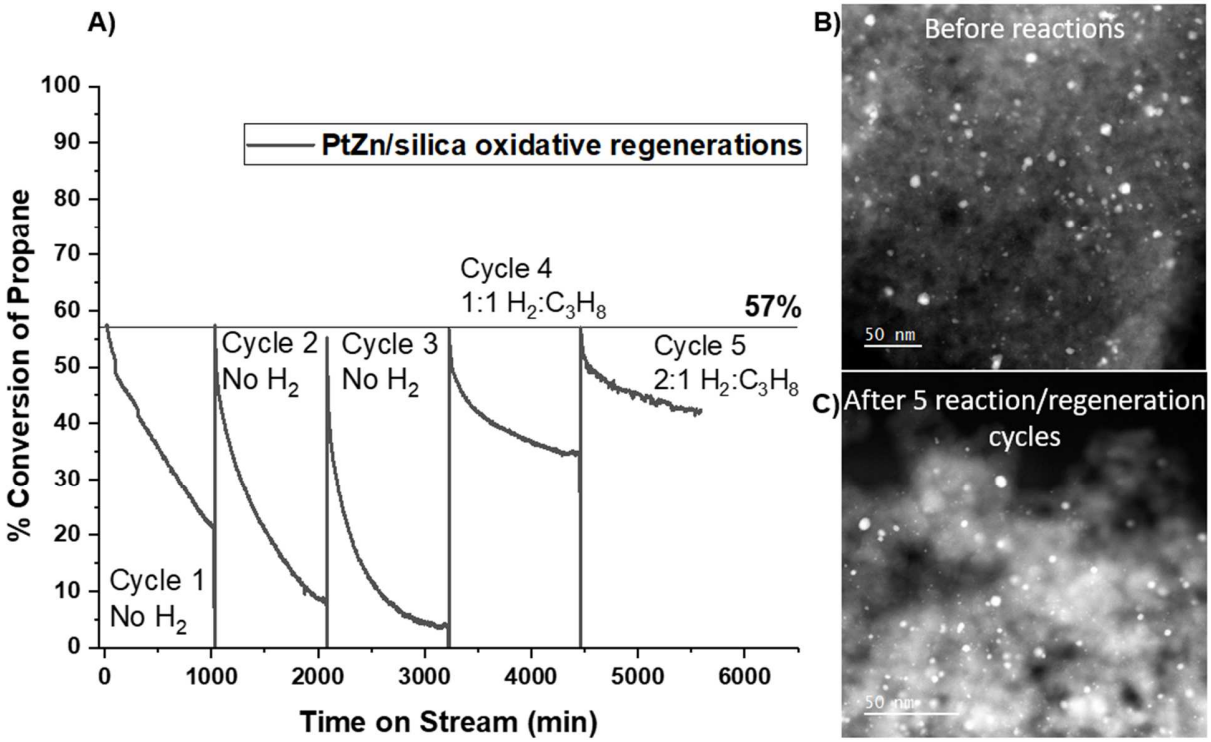

Figure 1. A) % Conversion as a function of time on stream for $PtZn/SiO_2$ in three sets of conditions: (1) 10% propane in Ar (cycles 1-3), (2) 10% propane and 10% H_2 in Ar (cycle 4),

and (3) 10% propane and 20% H_2 in Ar (cycle 5). The reaction was carried out isothermally at 550 °C. At the end of each run (except the last), the catalyst was regenerated in air (40 mL/min) at 420 °C for 1 hr. B) HAADF STEM image of "as prepared" PtZn/SiO_2 pre-treated in H_2. C) HAADF STEM image of PtZn/SiO_2 after five 18-hr cycles followed by 1-hr regenerations using air at 420 °C (after cycle 5 without regeneration).

Next, we explored whether the activity could be recovered by *in situ* addition of H_2 to the feed after the catalyst had partially deactivated. A stream of 5% propane in Ar (40 mL/min total flow) was used for PDH using PtMn/SiO_2 (2%Pt, 5%Mn) at 550 °C. When H_2 was introduced after 150 minutes on stream in a ratio of H_2:C_3H_8 = 1, as shown in Figure 2A, the conversion increased with an accompanying shift in overall stability. A greater percentage, approaching 100%, of the initial activity could be recovered by starting the H_2 treatment at shorter times (60 minutes) on stream, as seen in a similar experiment in Figure S14. Figure 2A also provides the conversion versus time, final conversions, and equilibrium conversions for the initial part of the run without added H_2. Conversion and selectivity are defined in Equations S1-S3. There is a dramatic contrast for selectivity between the "coking" conditions, i.e. without H_2, and the "non-coking conditions", i.e. co-fed H_2. We achieve conversions closer to equilibrium upon the addition of cofed H_2, which is consistent with literature [13]. Figure 2B depicts a "pulsing" experiment with PtMn/SiO_2 which entails alternating periods of 20 min on stream in coking conditions (40 mL/min of 5% propane in Ar) and 20 min with pure H_2 flow (40 mL/min). 20-minute pulses were chosen based on the data in Figure S14 which suggest that H_2 regeneration is more impactful after less time on stream. After two regenerations with pure H_2, the high activity, gas phase selectivity, and total selectivity are comparable to those parameters for the fresh catalyst. During the H_2 regeneration process, no gas phase products are observed via the MicroGC, suggesting either that the amounts of carbon deposited on the NPs are too small to be detected or that the coke cannot be reacted away in H_2 presumably because most of it is located on the support [60].

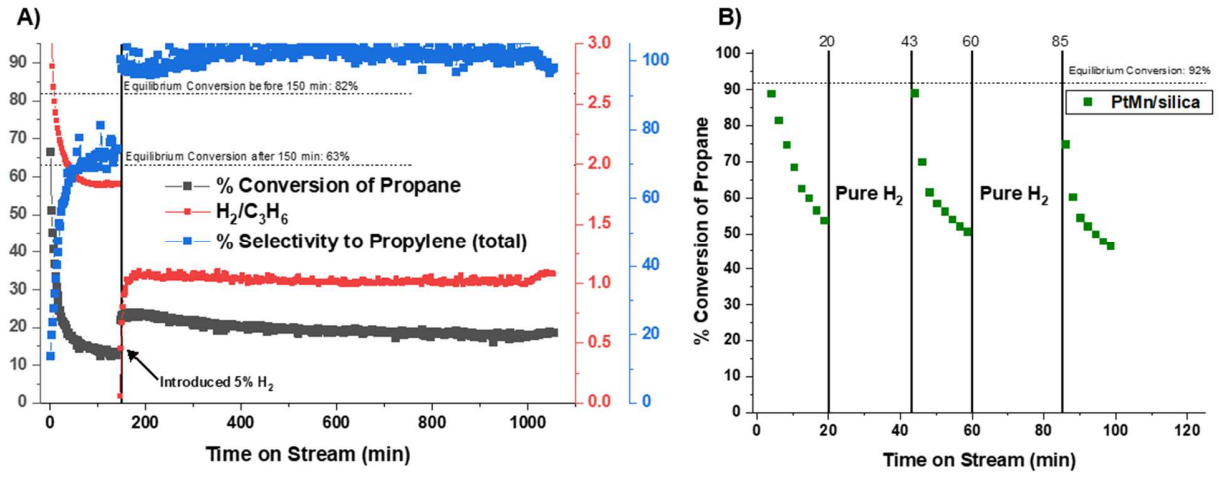

Figure 2. A) % Conversion of propane (black), % propylene selectivity (blue), and H_2/C_3H_6 (red) as a function of time on stream for 60 mg of $PtMn/SiO_2$. The reaction was carried out isothermally at 550 °C. The feed is initially 5% propane in Ar with a total flow rate of 40 mL/min. At a time on stream of 150 min, 5% H_2 was introduced, making the feed 5% propane, 5% H_2, and 90% Ar with a total flowrate of 40 mL/min. B) % Conversion vs time on stream for 60 mg of $PtMn/SiO_2$. Reaction cycles (green squares) of 20 mins on stream with 5% propane in N_2 and 20 mins with pure H_2 flowing over the catalyst with a total flow rate of 40 mL/min. The reaction and H_2 pulsing were carried out isothermally at 600°C.

To further investigate the nature of the coke on a fully deactivated catalyst, 60 mg of $PtZn/SiO_2$ catalyst was run for 40 hours on stream under coking conditions of 5% propane in argon (40 mL/min total flow rate). In Figure 3, HRTEM images and the TGA profile of the spent $PtZn/SiO_2$ catalyst that has nearly completely deactivated by coking are shown. Figure 4 shows that multi-layer graphitic carbon is present all over the support and possibly on the nanoparticles. Nevertheless, the surface of the nanoparticles cannot be directly imaged because of overlap with the silica support. Previous work done by Pham *et al.* [61,62] reported images of monolayers of carbon on a silica support. Comparing with those images, it becomes clear that we have multilayer carbon on this sample based on the crystalline lattice fringes at the edge of the silica that can be indexed to the graphite (002) planes. This multilayer carbon comprises about 23 wt % of the entire sample ($PtZn/SiO_2$) based on TGA measurement in air. Redekop *et al.* [63] describe a similar situation with multilayer crystalline carbon that forms all over the catalyst and catalyst support for a $Pt/Mg(Al)O_x$ catalyst material.

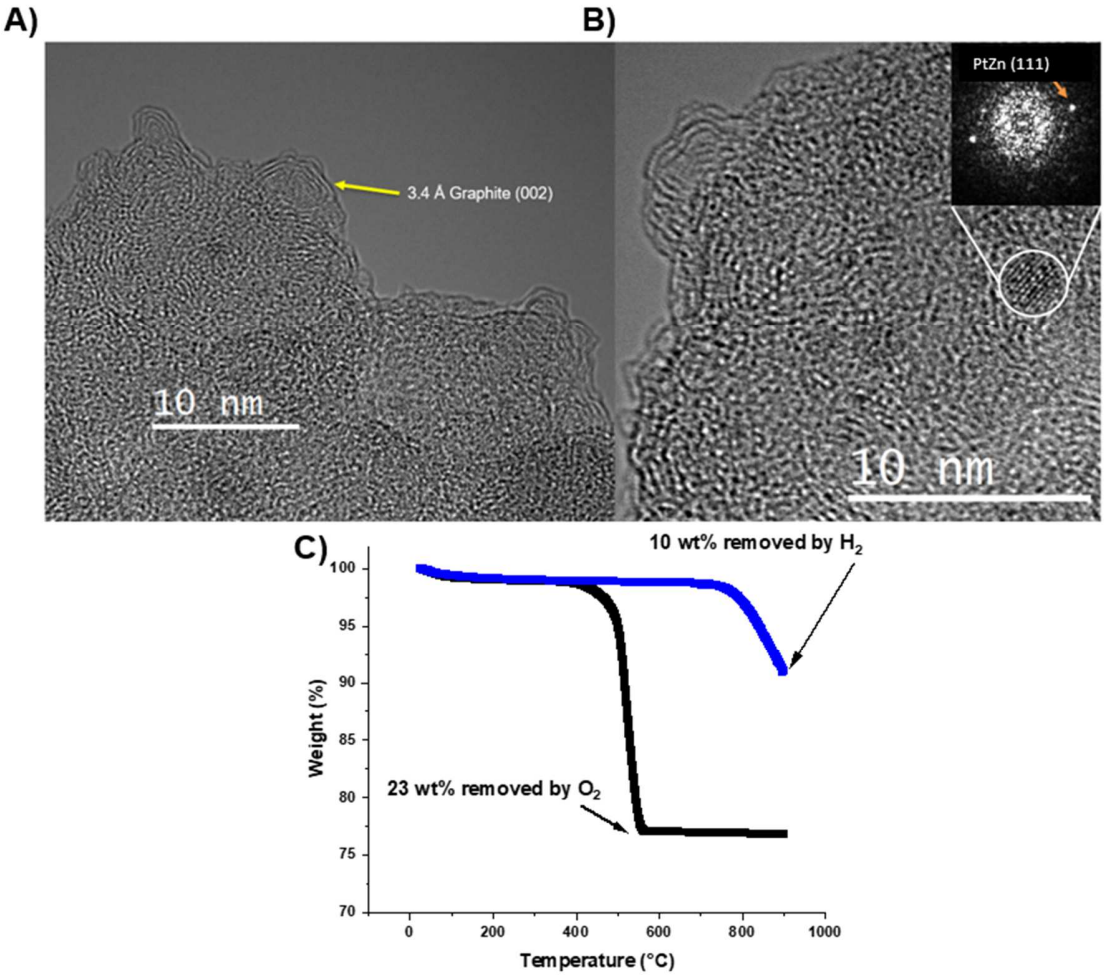

Figure 3. (A and B) HRTEM images of $PtZn/SiO_2$ after 40 hours on stream with a 5% propane in Ar feed. (C) TGA profile of this deactivated $PtZn/SiO_2$ catalyst when heated in air (black) and 4% H_2 in N_2 (blue).

Having established the role of cofed H_2 on the $PtMn/SiO_2$ and $PtZn/SiO_2$ catalysts, conditions that would lead to longer lifetimes were investigated. Figure 4A depicts the performance of $PtSn/SiO_2$ at 600 °C while feeding 100 mL/min of 55% propane 40% H_2 and 5% N_2. The catalyst is stable for 5 days on stream operating initially at 97% of equilibrium conversion and dropping after 120 hours to 77% of equilibrium. The fact that the total selectivity and the gas phase selectivity are similar suggests there is minimum coking or cracking side reactions under these operating conditions. It was found that, in the presence of sufficient H_2, the $PtSn/SiO_2$ catalyst effectively circumvents cracking and coking, leading to exceptionally good

stability near equilibrium conversion. Figure 4B shows that the PtMn/SiO_2 catalyst achieves similar stable long-term performance in the presence of co-fed H_2.

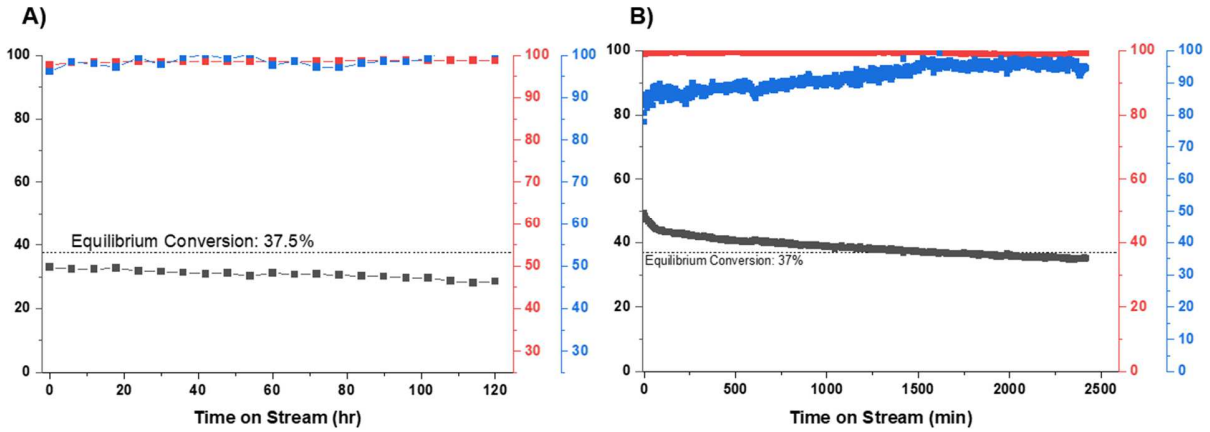

Figure 4. % Conversion (black), % Gas phase selectivity (red), and % total selectivity (blue) as a function of time on stream for A) 250 mg of PtSn/SiO_2 at 600 °C in 55% propane 5% N_2 and 45% H_2. B) 60 mg PtMn/SiO_2 at 600 °C (furnace set point) in 45% propane 45% H_2 and 10% H_2.

To explore whether the coke migration from the Pt alloy NPs onto the SiO_2 support was responsible for the stability observed with cofed H_2, *in situ* temperature programmed oxidations (TPO) were performed. After the reaction, the catalyst is cooled to 40 °C, purged with N_2, and then reacted *in situ* using 40 mL/min of 10% O_2 in N_2 while the furnace ramped to 650 °C at 10 °C/min. Figure 5 shows the TPO profiles for PtMn/SiO_2 catalysts that have seen a 0:1 and 1:1 H_2:C_3H_8 feed ratios for different amounts of time and reaction conditions (coking versus non-coking). Figure 5A shows that coking conditions for 15 hours results in the largest amount of coke that is also the most difficult to remove as evidenced by the higher temperature required to fully oxidize the coke. The presence of two peaks in the spectra suggests that there are two types of coke, one which is oxidized at low temperature (~ 350 °C) and one at a higher temperature (~ 450 °C). Applying coking conditions for less time (30 minutes) results in the formation of less coke, which can also be removed at a lower temperature. Under non-coking conditions, which includes co-feeding H_2 for 30 minutes, we see the least amount of coke deposited. Both the low temperature coke as well as the high temperature coke is reduced as seen from the pink versus the black curves in Figure 5A. Figure 5B illustrates that an additional H_2 treatment for 30 minutes after use in coking reaction conditions for 30 minutes results in the removal of some

coke, and the coke that remains is more easily removed by oxidation as evidenced by the lower temperature required.

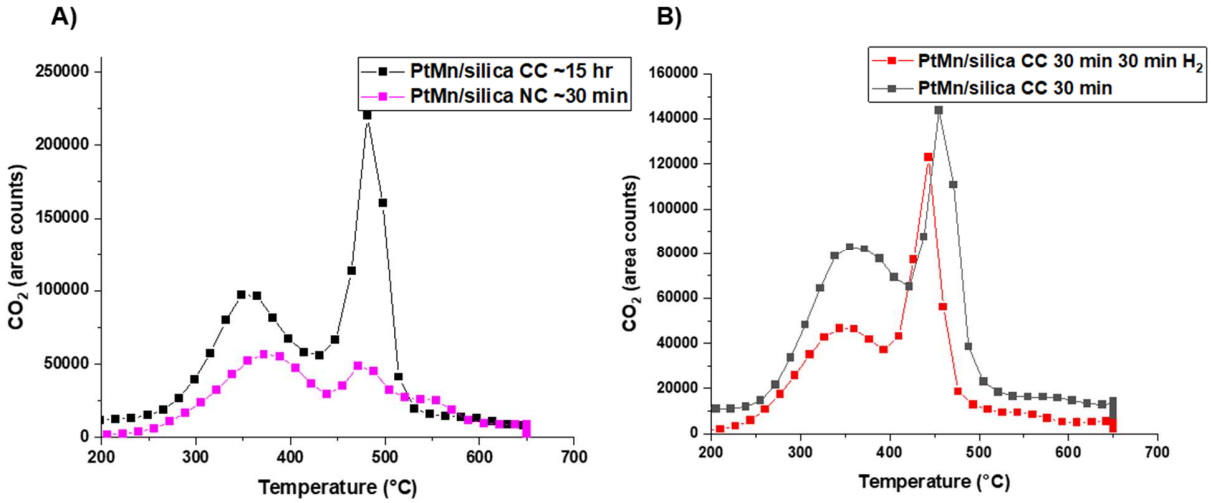

Figure 5. A) TPO profile of a $PtMn/SiO_2$ catalyst after 15 hr in coking conditions (5% propane in Ar) at 550 °C, cooled in the reaction atmosphere, purged with nitrogen at room temperature, and then exposed to 40 mL/min of 10% O_2 in N_2 by heating at 10°C/min to 650 °C and then held for 30 min. The same procedure was performed for separate $PtMn/SiO_2$ samples (60 mg) that had seen coking conditions for 30 min and non-coking conditions (45% propane 45% H_2 & 10% N_2) for 30 min. B) Direct comparison of the coke deposited on $PtMn/SiO_2$ after coking conditions for 30 min with and without an additional 30 min H_2 treatment (also cooled in H_2 instead of reaction conditions).

3. Discussion

Figure 1 shows that the $PtZn/SiO_2$ catalyst can be oxidatively regenerated via treatment in air at 420°C for at least one hour. The loss of activity becomes more rapid with each successive reaction cycle, suggesting that the regenerated catalyst is different from the initial catalyst. With each new reaction cycle, coke accumulation is seen to occur more rapidly, perhaps due to the residual coke left after incomplete burn-off. The residual coke may cause more facile nucleation and growth of freshly deposited coke. The reactions in Figure 1 were run in 40 mL/min of 10% propane in inert, but at a lower partial pressure of propane, the deactivation is even more pronounced. For example, experiments at 5% propane in Ar show even more precipitous drops in conversion as a function of time as seen in Figure S18. Despite the

incomplete removal of coke species, the catalyst can be restored to its initial conversion and can even operate in a stable manner with co-fed H_2, as is shown in cycle 4 and 5. The STEM image of the catalyst in Figure 1 showed no increase in particle size after the reaction cycles, suggesting that silica supported catalysts can be successfully regenerated by oxidation at low temperature.

A study of this reaction with temporal analysis of products (TAP) [63] had elucidated many of the phenomena on a $Pt/Mg(Al)O_x$ catalyst that we also see with Pt alloys on silica. The study concludes that the most active sites are rapidly covered by coke during the initial exposure of the catalyst to propane. It also concludes that graphene-like layers are formed on and near the catalyst support and that the TPO profiles can be interpreted in terms of coke present on the metal and coke present on the support [63]. When the reactants are passed over the catalyst in pulses, alternating with an inert gas, a modest increase in propylene production was observed for a short period of time. This increase in conversion is attributed to an additional transport process whereby coke precursors migrate away from the catalyst NPs. The increase in activity, by means of time on stream in inert, is short lived and not necessarily useful from an operational perspective. In this work, we show that the transport process that allows coke to migrate away from the surface is accelerated in the presence of pure H_2 and that this can be used as a regeneration strategy to stave off the need for oxidative regeneration.

Figure 2A shows that for a coke-deactivated catalyst, addition of H_2 to the feed stream not only leads to a sudden increase in the conversion, but also leads to a much slower deactivation rate. Thus, H_2 not only leads to the recovery of active sites but slows the deactivation rate upon its continuous feeding thereafter. This closer approach to equilibrium for both ethane and propane has been reported in literature [12,13]. However, the spontaneous recovery of catalyst activity and selectivity of a coked catalyst accelerated by the presence of H_2 has not been reported in the literature for silica-supported catalysts. Figure 2B shows that if a catalyst is coked for a shorter time, the initial conversion can be nearly restored. Similar observations were reported in a TAP reactor study describing the pulsing of reactants and then waiting at the reaction temperature for the next pulse; nonetheless, the recovery in performance was not significant from an applied perspective [63]. There is also a comparative study detailing similar regeneration treatments using H_2 and N_2 for a $PtSn/Al_2O_3$ catalyst and arrived at the conclusions that the mobility of coke is “activated” in the presence of H_2 [50]. In this work, we

show that initial activity can be recovered using H_2 alone if done early and frequently enough on silica supported Pt alloys. It can be seen from Figure S16 that regeneration in N_2 at the reaction temperature allows one to operate at the same conversion with each cycle because of a similar mechanism involving coke mobility from NP to support. However, the assessed coke mobility is not as pronounced because it is not "activated" like it is in the presence of H_2.

As shown in Figure 3 for a $PtZn/SiO_2$ catalyst that was highly deactivated, we observe graphitic carbon (identified from the lattice fringes) in all regions of the catalyst including both the metal and the support. TGA in flowing air shows a weight loss indicating that about 23 wt% of coke had accumulated on the catalyst. For the same sample, TGA in H_2 surprisingly indicated that slightly less than half as much coke could be removed relative to the TGA done in air. It should be noted that a non-zero amount of weight loss is observed during TGA (dilute H_2) at reaction conditions, suggesting that there is some degree of coke hydrogenation that is difficult to detect. Attempts to characterize the species that may be reacting via hydrogenation using TPR-MS or by MicroGC analysis are inconclusive. Nonetheless, the TGA conducted in dilute H_2 suggests some coke species may be liberated by hydrogenation depending on the type and location of said coke. This observation is also evidenced by the *in situ* TPO data discussed later.

Figure 4 demonstrates the stability one can achieve by cofeeding H_2 in large enough amounts (~1:1 with propane). The mechanistic aspects of mitigating coke deactivation (suppression) by cofeeding hydrogen for propane dehydrogenation have been well established. Saerens et al [12] proposed that H_2 competes with coke precursors (i.e., CCH_3 ethylidyne and CH methylidyne) for active sites, decreases the adsorption strength of propylene, and increases the energy barrier for coke producing side reactions. This explanation appears to agree with the findings from Figure 1, which illustrates the stabilization of the catalyst with co-fed H_2; still, it should be noted that H_2 does not completely prevent coking, and coke mobility or location may also play a significant role in catalyst stability. Eventually, all catalysts deposit enough coke to lead to a loss of activity and require regeneration to restore activity. Therefore, the regenerability of the catalyst is paramount to successful implementation in industrial processes.

In Figure 5, temperature programed oxidation of the coke shows that there are two types of coke, which oxidize at different temperatures. Since Pt is a highly effective oxidation catalyst, it

is likely that the coke removed at a lower temperature is on or near the Pt alloy NPs while the coke removed at a higher temperature resides on the support. In Figure 5A, for a $PtMn/SiO_2$ catalyst run in propane alone (low concentration) for 30 min and 15 h, the amount of coke on the alloy NPs is very similar (compare both black curves in Figure 5), while there is much more coke on the support when reacted for a longer reaction time. Although longer reaction times lead to more coke on the support, the increase is not linearly proportional with reaction time. Approximately as much coke is deposited in the first 30 min as the next 14+ hours (compare both black curves in Figure 5). Thus, coke deposition on the metal NPs is rapid and doesn't change much at longer times, while the coke on the support deposits quickly during the first few minutes and more slowly at longer times. Treatment of this catalyst in H_2, Figure 5B, suggests that a significant amount of coke on the metal NP is removed, which is consistent with an increase in conversion observed in Figures 2 and 5. The amount of coke on the support, i.e., the high temperature coke, however, is little changed, see Figure 5A (blue and red squares, 30 min with and without H_2) and Figure 5B. Thus, once the coke on the support has formed, it is not readily removed by H_2.

While Figure 2B shows that for short reaction times the initial activity can be restored by H_2 regeneration, the TPO in Figure 5 suggests that H_2 regeneration is not a viable approach after a long-term reaction. This is because while H_2 regeneration will remove coke from the metallic NPs, it is not able to remove coke from the support, which will accumulate over long periods of time on stream and eventually deactivate the active surface of the catalyst which necessitates oxidative regeneration. A more effective strategy may be to co-feed propane and H_2 to limit the amount of coke on the metal NP and support and mitigate the deactivation obtaining longer on-stream operation, as seen in Figure 4 or Figure S17. Low temperature oxidation effectively removes the carbon from the metallic NPs, but longer oxidative regeneration times or higher temperature are required to completely remove coke from the support. By co-feeding propane and H_2, the amount of coke on the support can be suppressed; thus, low temperature oxidation will be effective at removing all the coke and restoring the catalyst performance. The low temperature regeneration will also lead to long-term operation since the NPs do not sinter at these lower temperatures (Figure 1B). With low coke on catalysts, it is also possible to use higher oxygen concentrations since the oxidation exotherms will be much less pronounced.

4. Conclusions

The addition of H_2 has a clear stabilizing effect on silica supported Pt alloys in PDH consistent with established literature. In the absence of co-fed H_2, propane dehydrogenation leads to rapid coking of the metallic NPs and the silica support. Coke formation on the metallic NPs occurs in the first 30 min with little additional coke added at longer reaction times. Coking on the support also occurs rapidly during the first 30 min but continues to increase with increasing reaction time. Complete loss of conversion occurs at coke levels of about 25%. Oxidative regeneration at 420 °C does not sinter the metallic NPs and restores the initial conversion; however, with each successive reaction cycle, the deactivation rate becomes more rapid, suggesting that not all the coke has been removed from the catalyst. Treatment with H_2 or co-feeding H_2 partially or fully restores coke-deactivated catalysts if applied after short reaction cycles. Co-fed H_2 lowers the overall deactivation rate while allowing a closer approach to equilibrium and higher overall conversion. Analysis of the coked catalysts suggests there are two types of coke, i.e., on the metal NPs and on the support. The oxidation of the coke on the metal NPs occurs at a lower temperature compared to the coke on the support. Treatment in H_2 lowers the coke on the metal NPs but does not reduce the amount of coke present on the support. High partial pressures of co-fed H_2, however, are effective at significantly lowering the amount of coke on the support. Thus, by co-feeding H_2 and propane, lower deactivation is achieved, and longer reaction cycles are possible. Maintaining low coke amounts on the support allows low temperature oxidative regeneration to effectively remove all the coke from the catalyst, restoring the initial activity and enabling long-term performance.

In addition to being chemically inert, as we show in this study, silica provides a reservoir for coke species that appear to migrate away from the catalytically active metal nanoparticles, helping to maintain dehydrogenation activity for longer periods of time.

5. Acknowledgements

This work was supported by NSF/ERC CISTAR, which is supported by the National Science Foundation under Cooperative Agreement No. EEC-164772. Acquisition of the TEM was supported by the NSF MRI Grant DMR-1828731. The research used resources at the 8-ID beamline of the National Synchrotron Light Source II, a US Department of Energy Office of

Science User Facility operated by Brookhaven National Laboratory under contract no. DE-SC0012704. Use of the Advanced Photon Source, a US Department of Energy Office of Basic Energy Sciences, was supported under contract no. DE-AC02-06CH11357. The MRCAT beamline 10-BM is supported by the Department of Energy as well as the MRCAT member institutions.

References

[1] U.S. Energy Information Administration. Annual Energy Outlook 2022; U.S. Energy Information Administration: 2022.
[2] E. National Academies of Sciences, The Changing Landscape of Hydrocarbon Feedstocks for Chemical Production: Implications for Catalysis: Proceedings of a Workshop, 2016. https://doi.org/10.17226/23555.
[3] Q. Wang, R. Li, Research status of shale gas: A review, Renew. Sustain. Energy Rev. 74 (2017) 715–720. https://doi.org/10.1016/j.rser.2017.03.007.
[4] T. Ridha, Y. Li, E. Gençer, J.J. Siirola, J.T. Miller, F.H. Ribeiro, R. Agrawal, Valorization of Shale Gas Condensate to Liquid Hydrocarbons through Catalytic Dehydrogenation and Oligomerization, Processes. 6 (2018) 139. https://doi.org/10.3390/pr6090139.
[5] S. Chen, X. Chang, G. Sun, T. Zhang, Y. Xu, Y. Wang, C. Pei, J. Gong, Propane dehydrogenation: catalyst development, new chemistry, and emerging technologies, Chem. Soc. Rev. 50 (2021) 3315–3354. https://doi.org/10.1039/D0CS00814A.
[6] J.J.H.B. Sattler, J. Ruiz-Martinez, E. Santillan-Jimenez, B.M. Weckhuysen, Catalytic Dehydrogenation of Light Alkanes on Metals and Metal Oxides, Chem. Rev. 114 (2014) 10613–10653. https://doi.org/10.1021/cr5002436.
[7] H.N. Pham, J.J.H.B. Sattler, B.M. Weckhuysen, A.K. Datye, Role of Sn in the Regeneration of Pt/γ-Al2O3 Light Alkane Dehydrogenation Catalysts, ACS Catal. 6 (2016) 2257–2264. https://doi.org/10.1021/acscatal.5b02917.
[8] Y. Dai, X. Gao, Q. Wang, X. Wan, C. Zhou, Y. Yang, Recent progress in heterogeneous metal and metal oxide catalysts for direct dehydrogenation of ethane and propane, Chem. Soc. Rev. 50 (2021) 5590–5630. https://doi.org/10.1039/D0CS01260B.
[9] Shaping the future of on-purpose propylene production, (n.d.). https://www.hydrocarbonprocessing.com/magazine/2017/april-2017/special-focus-petrochemical-developments/shaping-the-future-of-on-purpose-propylene-production (accessed December 19, 2022).
[10] J. Wang, X. Chang, S. Chen, G. Sun, X. Zhou, E. Vovk, Y. Yang, W. Deng, Z.-J. Zhao, R. Mu, C. Pei, J. Gong, On the Role of Sn Segregation of Pt-Sn Catalysts for Propane Dehydrogenation, ACS Catal. 11 (2021) 4401–4410. https://doi.org/10.1021/acscatal.1c00639.
[11] Y. Zhu, Z. An, H. Song, X. Xiang, W. Yan, J. He, Lattice-Confined Sn (IV/II) Stabilizing Raft-Like Pt Clusters: High Selectivity and Durability in Propane Dehydrogenation, ACS Catal. 7 (2017) 6973–6978. https://doi.org/10.1021/acscatal.7b02264.
[12] S. Saerens, M.K. Sabbe, V.V. Galvita, E.A. Redekop, M.-F. Reyniers, G.B. Marin, The Positive Role of Hydrogen on the Dehydrogenation of Propane on Pt(111), ACS Catal. 7 (2017) 7495–7508. https://doi.org/10.1021/acscatal.7b01584.

[13]G. Siddiqi, P. Sun, V. Galvita, A.T. Bell, Catalyst performance of novel Pt/Mg(Ga)(Al)O catalysts for alkane dehydrogenation, J. Catal. 274 (2010) 200–206. https://doi.org/10.1016/j.jcat.2010.06.016.
[14]V. Galvita, G. Siddiqi, P. Sun, A.T. Bell, Ethane dehydrogenation on Pt/Mg(Al)O and PtSn/Mg(Al)O catalysts, J. Catal. 271 (2010) 209–219. https://doi.org/10.1016/j.jcat.2010.01.016.
[15]J. Wu, S. Mallikarjun Sharada, C. Ho, A.W. Hauser, M. Head-Gordon, A.T. Bell, Ethane and propane dehydrogenation over PtIr/Mg(Al)O, Appl. Catal. Gen. 506 (2015) 25–32. https://doi.org/10.1016/j.apcata.2015.08.029.
[16]A.H. Motagamwala, R. Almallahi, J. Wortman, V.O. Igenegbai, S. Linic, Stable and selective catalysts for propane dehydrogenation operating at thermodynamic limit, Science. 373 (2021) 217–222. https://doi.org/10.1126/science.abg7894.
[17]B. Frank, T.P. Cotter, M.E. Schuster, R. Schlögl, A. Trunschke, Carbon Dynamics on the Molybdenum Carbide Surface during Catalytic Propane Dehydrogenation, Chem. – Eur. J. 19 (2013) 16938–16945. https://doi.org/10.1002/chem.201302420.
[18]C.-F. Li, X. Guo, Q.-H. Shang, X. Yan, C. Ren, W.-Z. Lang, Y.-J. Guo, Defective TiO2 for Propane Dehydrogenation, Ind. Eng. Chem. Res. 59 (2020) 4377–4387. https://doi.org/10.1021/acs.iecr.9b06759.
[19]J.J.H.B. Sattler, A.M. Beale, B.M. Weckhuysen, Operando Raman spectroscopy study on the deactivation of Pt/Al2O3 and Pt–Sn/Al2O3 propane dehydrogenation catalysts, Phys. Chem. Chem. Phys. 15 (2013) 12095–12103. https://doi.org/10.1039/C3CP50646K.
[20]Y. Li, Y. Ma, Q. Zhang, V.A. Kondratenko, G. Jiang, H. Sun, S. Han, Y. Wang, G. Cui, M. Zhou, Q. Huan, Z. Zhao, C. Xu, G. Jiang, E.V. Kondratenko, Molecularly defined approach for preparation of ultrasmall Pt-Sn species for efficient dehydrogenation of propane to propene, J. Catal. 418 (2023) 290–299. https://doi.org/10.1016/j.jcat.2023.01.027.
[21]R.A. Meyers, W. Spieker, G.J. Nedohin, Handbook of Petroleum Refining, 4th ed., McGraw-Hill, 2016.
[22]C.-W. Chang, H.N. Pham, R. Alcala, A.K. Datye, J.T. Miller, Dehydroaromatization Pathway of Propane on PtZn/SiO2 + ZSM-5 Bifunctional Catalyst, ACS Sustain. Chem. Eng. 10 (2022) 394–409. https://doi.org/10.1021/acssuschemeng.1c06579.
[23]H. Xiong, S. Lin, J. Goetze, P. Pletcher, H. Guo, L. Kovarik, K. Artyushkova, B.M. Weckhuysen, A.K. Datye, Thermally Stable and Regenerable Platinum–Tin Clusters for Propane Dehydrogenation Prepared by Atom Trapping on Ceria, Angew. Chem. 129 (2017) 9114–9119. https://doi.org/10.1002/ange.201701115.
[24]S. Chen, Z.-J. Zhao, R. Mu, X. Chang, J. Luo, S.C. Purdy, A.J. Kropf, G. Sun, C. Pei, J.T. Miller, X. Zhou, E. Vovk, Y. Yang, J. Gong, Propane Dehydrogenation on Single-Site [PtZn4] Intermetallic Catalysts, Chem. 7 (2021) 387–405. https://doi.org/10.1016/j.chempr.2020.10.008.
[25]V.J. Cybulskis, B.C. Bukowski, H.-T. Tseng, J.R. Gallagher, Z. Wu, E. Wegener, A.J. Kropf, B. Ravel, F.H. Ribeiro, J. Greeley, J.T. Miller, Zinc Promotion of Platinum for Catalytic Light Alkane Dehydrogenation: Insights into Geometric and Electronic Effects, ACS Catal. 7 (2017) 4173–4181. https://doi.org/10.1021/acscatal.6b03603.
[26]Z. Wu, B.C. Bukowski, Z. Li, C. Milligan, L. Zhou, T. Ma, Y. Wu, Y. Ren, F.H. Ribeiro, W.N. Delgass, J. Greeley, G. Zhang, J.T. Miller, Changes in Catalytic and Adsorptive Properties of 2 nm Pt3Mn Nanoparticles by Subsurface Atoms, J. Am. Chem. Soc. 140 (2018) 14870–14877. https://doi.org/10.1021/jacs.8b08162.

[27]C. Ye, M. Peng, Y. Wang, N. Zhang, D. Wang, M. Jiao, J.T. Miller, Surface Hexagonal Pt1Sn1 Intermetallic on Pt Nanoparticles for Selective Propane Dehydrogenation, ACS Appl. Mater. Interfaces. 12 (2020) 25903–25909. https://doi.org/10.1021/acsami.0c05043.
[28]Q. Sun, N. Wang, Q. Fan, L. Zeng, A. Mayoral, S. Miao, R. Yang, Z. Jiang, W. Zhou, J. Zhang, T. Zhang, J. Xu, P. Zhang, J. Cheng, D.-C. Yang, R. Jia, L. Li, Q. Zhang, Y. Wang, O. Terasaki, J. Yu, Subnanometer Bimetallic Platinum–Zinc Clusters in Zeolites for Propane Dehydrogenation, Angew. Chem. Int. Ed. 59 (2020) 19450–19459. https://doi.org/10.1002/anie.202003349.
[29]S.W. Han, H. Park, J. Han, J.-C. Kim, J. Lee, C. Jo, R. Ryoo, PtZn Intermetallic Compound Nanoparticles in Mesoporous Zeolite Exhibiting High Catalyst Durability for Propane Dehydrogenation, ACS Catal. 11 (2021) 9233–9241. https://doi.org/10.1021/acscatal.1c01808.
[30]N. Kaylor, R.J. Davis, Propane dehydrogenation over supported Pt-Sn nanoparticles, J. Catal. 367 (2018) 181–193. https://doi.org/10.1016/j.jcat.2018.09.006.
[31]L. Deng, Z. Zhou, T. Shishido, Behavior of active species on Pt-Sn/SiO2 catalyst during the dehydrogenation of propane and regeneration, Appl. Catal. Gen. 606 (2020) 117826. https://doi.org/10.1016/j.apcata.2020.117826.
[32]P. Wang, J. Yao, Q. Jiang, X. Gao, D. Lin, H. Yang, L. Wu, Y. Tang, L. Tan, Stabilizing the isolated Pt sites on PtGa/Al2O3 catalyst via silica coating layers for propane dehydrogenation at low temperature, Appl. Catal. B Environ. 300 (2022) 120731. https://doi.org/10.1016/j.apcatb.2021.120731.
[33]H. Jeong, O. Kwon, B.-S. Kim, J. Bae, S. Shin, H.-E. Kim, J. Kim, H. Lee, Highly durable metal ensemble catalysts with full dispersion for automotive applications beyond single-atom catalysts, Nat. Catal. 3 (2020) 368–375. https://doi.org/10.1038/s41929-020-0427-z.
[34]J.H. Kwak, J. Hu, D. Mei, C.-W. Yi, D.H. Kim, C.H.F. Peden, L.F. Allard, J. Szanyi, Coordinatively Unsaturated Al3+ Centers as Binding Sites for Active Catalyst Phases of Platinum on γ-Al2O3, Science. 325 (2009) 1670–1673. https://doi.org/10.1126/science.1176745.
[35]J.H. Kwak, J.Z. Hu, D.H. Kim, J. Szanyi, C.H.F. Peden, Penta-coordinated Al3+ ions as preferential nucleation sites for BaO on γ-Al2O3: An ultra-high-magnetic field 27Al MAS NMR study, J. Catal. 251 (2007) 189–194. https://doi.org/10.1016/j.jcat.2007.06.029.
[36]K. Searles, K.W. Chan, J.A. Mendes Burak, D. Zemlyanov, O. Safonova, C. Copéret, Highly Productive Propane Dehydrogenation Catalyst Using Silica-Supported Ga–Pt Nanoparticles Generated from Single-Sites, J. Am. Chem. Soc. 140 (2018) 11674–11679. https://doi.org/10.1021/jacs.8b05378.
[37]Z. Lian, C. Si, F. Jan, S. Zhi, B. Li, Coke Deposition on Pt-Based Catalysts in Propane Direct Dehydrogenation: Kinetics, Suppression, and Elimination, ACS Catal. 11 (2021) 9279–9292. https://doi.org/10.1021/acscatal.1c00331.
[38]N.M. Schweitzer, B. Hu, U. Das, H. Kim, J. Greeley, L.A. Curtiss, P.C. Stair, J.T. Miller, A.S. Hock, Propylene Hydrogenation and Propane Dehydrogenation by a Single-Site Zn2+ on Silica Catalyst, ACS Catal. 4 (2014) 1091–1098. https://doi.org/10.1021/cs401116p.
[39]B. Hu, N.M. Schweitzer, G. Zhang, S.J. Kraft, D.J. Childers, M.P. Lanci, J.T. Miller, A.S. Hock, Isolated FeII on Silica As a Selective Propane Dehydrogenation Catalyst, ACS Catal. 5 (2015) 3494–3503. https://doi.org/10.1021/acscatal.5b00248.

[40]S. Derossi, G. Ferraris, S. Fremiotti, E. Garrone, G. Ghiotti, M.C. Campa, V. Indovina, Propane Dehydrogenation on Chromia/Silica and Chromia/Alumina Catalysts, J. Catal. 148 (1994) 36–46. https://doi.org/10.1006/jcat.1994.1183.
[41]K. Searles, G. Siddiqi, O. V. Safonova, C. Copéret, Silica-supported isolated gallium sites as highly active, selective and stable propane dehydrogenation catalysts, Chem. Sci. 8 (2017) 2661–2666. https://doi.org/10.1039/C6SC05178B.
[42]Y. Nakaya, F. Xing, H. Ham, K. Shimizu, S. Furukawa, Doubly Decorated Platinum–Gallium Intermetallics as Stable Catalysts for Propane Dehydrogenation, Angew. Chem. Int. Ed. 60 (2021) 19715–19719. https://doi.org/10.1002/anie.202107210.
[43]F. Jiang, L. Zeng, S. Li, G. Liu, S. Wang, J. Gong, Propane Dehydrogenation over Pt/TiO2–Al2O3 Catalysts, ACS Catal. 5 (2015) 438–447. https://doi.org/10.1021/cs501279v.
[44]G. Sun, Z. Zhao, R. Mu, S. Zha, L. Li, S. Chen, K. Zang, J. Luo, Z. Li, S. Purdy, A. Kropf, J. Miller, L. Zeng, J. Gong, Breaking the scaling relationship via thermally stable Pt/Cu single atom alloys for catalytic dehydrogenation, Nat. Commun. 9 (2018). https://doi.org/10.1038/s41467-018-06967-8.
[45]G. Liu, L. Zeng, Z.-J. Zhao, H. Tian, T. Wu, J. Gong, Platinum-Modified ZnO/Al2O3 for Propane Dehydrogenation: Minimized Platinum Usage and Improved Catalytic Stability, ACS Catal. 6 (2016) 2158–2162. https://doi.org/10.1021/acscatal.5b02878.
[46]A. Iglesias-Juez, A.M. Beale, K. Maaijen, T.C. Weng, P. Glatzel, B.M. Weckhuysen, A combined in situ time-resolved UV–Vis, Raman and high-energy resolution X-ray absorption spectroscopy study on the deactivation behavior of Pt and PtSn propane dehydrogenation catalysts under industrial reaction conditions, J. Catal. 276 (2010) 268–279. https://doi.org/10.1016/j.jcat.2010.09.018.
[47]Y. Nakaya, J. Hirayama, S. Yamazoe, K. Shimizu, S. Furukawa, Single-atom Pt in intermetallics as an ultrastable and selective catalyst for propane dehydrogenation, Nat. Commun. 11 (2020) 2838. https://doi.org/10.1038/s41467-020-16693-9.
[48]J. Im, M. Choi, Physicochemical Stabilization of Pt against Sintering for a Dehydrogenation Catalyst with High Activity, Selectivity, and Durability, ACS Catal. 6 (2016) 2819–2826. https://doi.org/10.1021/acscatal.6b00329.
[49]J.-W. Jung, W.-I. Kim, J.-R. Kim, K. Oh, H.L. Koh, Effect of Direct Reduction Treatment on Pt–Sn/Al2O3 Catalyst for Propane Dehydrogenation, Catalysts. 9 (2019) 446. https://doi.org/10.3390/catal9050446.
[50]C. Sun, J. Luo, M. Cao, P. Zheng, G. Li, J. Bu, Z. Cao, S. Chen, X. Xie, A comparative study on different regeneration processes of Pt-Sn/γ-Al2O3 catalysts for propane dehydrogenation, J. Energy Chem. 27 (2018) 311–318. https://doi.org/10.1016/j.jechem.2017.09.035.
[51]K.P. de Jong, Deposition Precipitation, in: Synth. Solid Catal., John Wiley & Sons, Ltd, 2009: pp. 111–134. https://doi.org/10.1002/9783527626854.ch6.
[52]J.T. Miller, M. Schreier, A.J. Kropf, J.R. Regalbuto, A fundamental study of platinum tetraammine impregnation of silica: 2. The effect of method of preparation, loading, and calcination temperature on (reduced) particle size, J. Catal. 225 (2004) 203–212. https://doi.org/10.1016/j.jcat.2004.04.007.
[53]D. Leshchev, M. Rakitin, B. Luvizotto, R. Kadyrov, B. Ravel, K. Attenkofer, E. Stavitski, The Inner Shell Spectroscopy beamline at NSLS-II: a facility for in situ and operando X-ray absorption spectroscopy for materials research, J. Synchrotron Radiat. 29 (2022) 1095–1106. https://doi.org/10.1107/S160057752200460X.

[54]T. Ressler, WinXAS: a Program for X-ray Absorption Spectroscopy Data Analysis under MS-Windows, J. Synchrotron Radiat. 5 (1998) 118–122. https://doi.org/10.1107/S0909049597019298.
[55]J.J. Rehr, C.H. Booth, F. Bridges, S.I. Zabinsky, X-ray-absorption fine structure in embedded atoms, Phys. Rev. B. 49 (1994) 12347–12350. https://doi.org/10.1103/PhysRevB.49.12347.
[56]N.J. LiBretto, C. Yang, Y. Ren, G. Zhang, J.T. Miller, Identification of Surface Structures in Pt3Cr Intermetallic Nanocatalysts, Chem. Mater. 31 (2019) 1597–1609. https://doi.org/10.1021/acs.chemmater.8b04774.
[57]L.G. Cesar, C. Yang, Z. Lu, Y. Ren, G. Zhang, J.T. Miller, Identification of a Pt3Co Surface Intermetallic Alloy in Pt–Co Propane Dehydrogenation Catalysts, ACS Catal. 9 (2019) 5231–5244. https://doi.org/10.1021/acscatal.9b00549.
[58]Z. Gan, Z. Lu, M. Bunian, L.B. Lagria, C.L. Marshall, R.M. Banish, S. Lee, Y. Lei, Synthesis of Pt3Zn1 and Pt1Zn1 intermetallic nanocatalysts for dehydrogenation of ethane, Phys. Chem. Chem. Phys. (2023). https://doi.org/10.1039/D2CP04173A.
[59]L. Deng, T. Shishido, K. Teramura, T. Tanaka, Effect of reduction method on the activity of Pt–Sn/SiO2 for dehydrogenation of propane, Catal. Today. 232 (2014) 33–39. https://doi.org/10.1016/j.cattod.2013.10.064.
[60]L. Liwu, Z. Tao, Z. Jingling, X. Zhusheng, Dynamic process of carbon deposition on Pt and Pt–Sn catalysts for alkane dehydrogenation, Appl. Catal. 67 (1990) 11–23. https://doi.org/10.1016/S0166-9834(00)84428-0.
[61]H.N. Pham, A.E. Anderson, R.L. Johnson, K. Schmidt-Rohr, A.K. Datye, Improved Hydrothermal Stability of Mesoporous Oxides for Reactions in the Aqueous Phase, Angew. Chem. Int. Ed. 51 (2012) 13163–13167. https://doi.org/10.1002/anie.201206675.
[62]H.N. Pham, A.E. Anderson, R.L. Johnson, T.J. Schwartz, B.J. O'Neill, P. Duan, K. Schmidt-Rohr, J.A. Dumesic, A.K. Datye, Carbon Overcoating of Supported Metal Catalysts for Improved Hydrothermal Stability, ACS Catal. 5 (2015) 4546–4555. https://doi.org/10.1021/acscatal.5b00329.
[63]E.A. Redekop, S. Saerens, V.V. Galvita, I.P. González, M. Sabbe, V. Bliznuk, M.-F. Reyniers, G.B. Marin, Early stages in the formation and burning of graphene on a Pt/Mg(Al)Ox dehydrogenation catalyst: A temperature- and time-resolved study, J. Catal. 344 (2016) 482–495. https://doi.org/10.1016/j.jcat.2016.10.023.